RAA 2020 Vol. **20** No. **8**, 122(8pp) doi: 10.1088/1674–4527/20/8/122

http://www.raa-journal.org *http://iopscience.iop.org/raa*

Research in Astronomy and Astrophysics

The dying accretion and jet in a powerful radio galaxy of Hercules A

Lin-Hui Wu[1], Qing-Wen Wu[1], Jian-Chao Feng[2], Ru-Sen Lu[3,4] and Xu-Liang Fan[5]

[1] School of Physics, Huazhong University of Science and Technology, Wuhan 430074, China; *qwwu@hust.edu.cn*
[2] School of Physics and Electronic Science, Guizhou Normal University, Guiyang 550001, China
[3] Shanghai Astronomical Observatory, Chinese Academy of Science, Shanghai 200030, China
[4] Max-Planck-Institut für Radioastronomie, Auf dem Hügel 69, D-53121 Bonn, Germany
[5] School of Mathematics, Physics and Statistics, Shanghai University of Engineering Science, Shanghai 201620, China

Received 2020 March 16; accepted 2020 March 29

Abstract Hercules A (Her A) is one of a rare class of dying and transition-type objects, which has a pair of giant, powerful radio lobes and a weak radio core. We reduce and analyze the radio data of Her A that were observed by the Expanded Very Large Array (EVLA) during 2010-2011 at C band. The intensity distribution is very smooth along the edge of the lobe front and the intensity also sharply decreases at the edge, which supports that magnetic fields may play an important role in radio lobes. The spectrum of the weak core is very steep and the core flux becomes weaker by about ten percent when compared to what was observed twenty years ago, which suggest that the central engine is still dying quickly. Her A deviates a lot from the relation between [O III] luminosity and low-frequency 178 MHz luminosity ($L_{\rm O\ III} - L_{\rm 178MHz}$) as defined by other FR I/II sources. However, when only radio core emission is considered, it roughly follows an $L_{\rm O\ III} - L_{\rm 178\,MHz}$ correlation. This result supports that the black-hole accretion and large-scale jet in Her A did not evolve simultaneously, and indicates that although the large-scale jet is still powerful, the accretion and inner jet have changed into an inactive state. Based on the estimated Bondi accretion rate, we model the spectrum of Her A with a radiatively inefficient accretion flow and jet model.

Key words: black hole physics — galaxies: jets — radiation mechanisms: non-thermal — galaxies: magnetic fields — radio continuum: galaxies

1 INTRODUCTION

Active galactic nuclei (AGNs) are powered by gravitational energy released by accreting matter of the central supermassive black holes (SMBHs), which can be divided into quasi-stellar objects (QSOs), Seyfert galaxies, low-ionization nuclear emission-line galaxies (LINERs), radio galaxies, etc. The different types of AGNs are possibly caused by the different accretion rates and/or orientation effects (the so-called unification model, e.g., Urry & Padovani 1995). Bright QSOs and faint LINERs are believed to be powered by different accretion modes, where an optically thick, geometrically thin accretion disk (a Shakura-Sunyaev disk, SSD) and optically thin, geometrically thick advection-dominated accretion flow (ADAF) should exist in QSOs and LINERs respectively (e.g., Shakura & Sunyaev 1973; Narayan & Yi 1994, 1995; Yuan & Narayan 2014). A small fraction of AGNs are radio loud, which normally host relativistic jets. Fanaroff-Riley (FR) Is and FR IIs are one population of famous radio galaxies, which are classified based on the lack or presence of hotspots in their radio lobes. The sources with radio luminosity at 178 MHz below and above $\sim 2 \times 10^{25}\ {\rm W\,Hz^{-1}\,sr^{-1}}$ are generally FR I class and FR II class respectively (e.g., Fanaroff & Riley 1974). It was proposed that the different FR I/II morphologies may be caused by different ambient media surrounding the jet lobes (e.g., Gopal-Krishna & Wiita 2000). Later on, it was found that both the jet power and accretion power of FR Is are systematically lower than those of FR IIs, and the FR dichotomy may be caused by the different accretion modes and jet properties (e.g., Ghisellini & Celotti 2001; Wang et al. 2003; Wu & Cao 2008; Xu et al. 2009; Chen et al. 2015). Based on narrow emission lines, the radio galaxies were also classified into High-Excitation or Low-Excitation Radio Galaxies (HERGs or LERGs respectively), where the main diagnostic of high excitation is the luminosity of the [O III]λ5007 line (e.g., Laing et al. 1994; Buttiglione et al. 2010). Most FR Is are LERGs while most FR IIs belong to HERGs. It should be noted that there are also some exceptions (e.g., HE FR Is and LE FR IIs), which may correspond to the transition type of FR I/II galaxies (e.g., Buttiglione et al. 2010, 2011; Macconi et al. 2020). LERGs and HERGs normally have Eddington-scaled luminosities lower or higher than 1% respectively, and they should have different accretion modes (Fan & Wu 2019; Best & Heckman 2012).

Relativistic jets in AGNs are powered by their central SMBHs. The magnetic field should play a key role in generation, acceleration, collimation and energy dissipation of these jets (e.g., McKinney & Narayan 2007; Yuan et al. 2015; Zhang et al. 2015; Tchekhovskoy & Bromberg 2016). The jet should be initially magnetic energy dominated and the magnetic energy is converted into the jet kinetic energy during the acceleration process. An important fraction of the magnetic energy may still survive at pc, kpc or even Mpc scales of jets (e.g., Li et al. 2006; Nakamura et al. 2006; Diehl et al. 2008; Kronberg et al. 2011; Gan et al. 2017). The high-energy and very high-energy gamma-ray emission of the large-scale radio lobes do support this scenario, where the magnetic field can be constrained in kpc or even Mpc scale of jets (e.g., Hardee & Rosen 2002; Laing et al. 2006; Stawarz et al. 2005; Kataoka & Stawarz 2005; Persic & Rephaeli 2019, 2020). The polarization, Faraday rotation measure and intensity structures also provide clues for the intensity and structure of the magnetic field associated with extragalactic jets, which are widely explored in former works (e.g., Laing 1981; Hardee & Rosen 2002; Gizani & Leahy 2004; Laing et al. 2006; Clausen-Brown et al. 2011; Casadio et al. 2019; Prior & Gourgouliatos 2019).

Hercules A (Her A) is one of the brightest radio sources in the sky, which has classical FR II type double radio lobes with linear size around 500 kpc. The radio luminosity of Her A is higher than the dividing line of FR I/II dichotomy. However, the lobes lack compact hot spots like those found in other bright FR IIs. It should be noted that Her A is also not a typical FR I type radio galaxy (Dreher & Feigelson 1984). From optical observations, Buttiglione et al. (2010) defined Her A as an extreme low excitation radio galaxy (ELEG), while most FR IIs are HERGs. The X-ray emission in Her A is thought to be due to bremsstrahlung of the very high temperature intracluster medium, and no evident compact X-ray core has been reported yet (Gizani & Leahy 2004). Therefore, the structure of the radio lobes, the lack of compact X-ray core and the properties of optical emission lines suggest that Her A might be a transitional case of FR I/II (e.g., FR 1.5, Dreher & Feigelson 1984).

The study of Her A will help to understand the evolution of radio galaxies. In this work, we present the radio properties of the jet in Her A based on high sensitivity data obtained from the Expanded Very Large Array (EVLA). We also explore the physical properties of the core region based on an accretion-jet model. In Sections 2 and 3, we describe and present the radio data reduction and the main results respectively. Discussion and conclusion are presented in Section 4. In this work, we adopt the spectral index, κ, as $S_\nu \propto \nu^{-\kappa}$ and $M_{\rm BH} = 2.5 \times 10^9\, M_\odot$ as the mass of the SMBH in Her A (Fujita et al. 2016). The redshift is $z = 0.154$ (Gizani & Leahy 2004), where 1 arcsec corresponds to 2.5 kpc by assuming the cosmological parameters of $H_0 = 70\,\rm km\,s^{-1}\,Mpc^{-1}$ and $\Omega_{\rm m} = 0.3$.

2 DATA REDUCTION

Her A was observed with the A, B and C configurations at C band by the EVLA during 2010–2011 (see Table 1). We extract the EVLA data from the NRAO data archive[1]. Data reduction was performed using standard reduction techniques in CASA[2], the Common Astronomy Software Applications package. All data sets were calibrated applying 3C 286 as the flux calibrator and bandpass calibrator, and utilizing J1651+0129 as the phase calibrator. We simply describe the data reduction as follows. Firstly, we examine the data set and flag the bad data, then we do a prior calibration, which contains antenna position correction, gain curve calibration and opacity correction. After that, we do delay calibration followed by bandpass calibration, and we set the flux density scale by SETJY for 3C 286. We perform phase calibration and complex gain calibration, and scale the flux density of J1651+0129 by FLUXSCALE. Finally, we apply the calibration by APPLYCAL and perform self-calibration for the target source (Her A). We note that data flagging and radio-frequency interference flagging are carried out during the whole calibration process. After proper self-calibration, we combine all the data sets by CONCAT. We image the source by TCLEAN in multi-scale, multi-term, multi-frequency mode with nterms = 2, and the task IMPBCOR was employed to produce the intensity and spectral index image with the reference frequency at 5 GHz. The noise level of the resultant intensi-

[1] The National Radio Astronomy Observatory (NRAO) is a facility of the National Science Foundation operated under cooperative agreement by Associated Universities, Inc. (*https://archive.nrao.edu*).

[2] *https://casaguides.nrao.edu/index.php/Karl_G._Jansky_VLA_Tutorial*, see also McMullin et al. (2007)

Table 1 VLA Observation of Her A

Date	Configuration	spws	Frequency range (MHz)
2010 Oct 17	C	14	4208–6000
2011 Mar 01	B	14	4208–6000
2011 Mar 27	B	14	4208–6000
2011 Sep 10	A	14	4208–6000

ty image is $\sigma_{\rm I} = 17\mu{\rm Jy\,beam^{-1}}$ and the resolution is 0.73×0.70 arcsec. We also image the data in 'cube' spectral mode with the same resolution, and perform Gaussian fitting for the core component at each spectral window (spw). Since the core is unresolved at any spw, we take the noise level as the flux error for each spw.

3 RESULTS

Figure 1 displays the intensity distribution for Her A at 5 GHz, where two large-scale jets with prominent rings, bridges and lobes are evident. The intensity distribution along the lobe front is very smooth. We further highlight the intensity distribution of the two selected slices that lie at the front edge of the west lobe in Figure 2. These two representative slices are selected from the lobe front (upper left panel) and backward region (lower left panel) respectively. It can be ascertained that the intensity distribution along the selected slice is very sharp at the edge in the lobe front. We calculate the slopes of the intensity variation against the distance along the selected slices with an interval of 0.4 arcsec (right panels of Fig. 2). The slopes are around 0 in the middle region of the selected slice and increase at the lobe edge, which means a sharp decrease in the intensity towards the lobe edge (in particular for the case of lobe front).

The total flux of Her A is 10.3 ± 0.3 Jy and the core flux is 8.8 ± 0.1 mJy at 5 GHz. Table 2 presents the results of Gaussian model fitting of the core component at each spw. The core flux varies from 10.4 mJy to 6.4 mJy from 4.27 GHz to 5.93 GHz. The radio core emission observed by EVLA is a little bit higher than that observed by the higher-resolution European VLBI Network (EVN), which suggests the Her A core is still diffuse at kpc scale (Gizani & Garrett 2002). Figure 3 presents the distribution of spectral index at the resolution of 0.73×0.70 arcsec (upper panel) and its error (lower panel), which are derived from the frequency range between 4.2 GHz and 6.0 GHz. The spectrum of the whole source is very steep with an averaged spectral index of $\kappa_{\rm total} \sim 2.2 \pm 0.3$. The distribution of the spectral index is quite similar to that of the intensity distribution, where the spectrum becomes steeper from the inner jet to lobe front. The spectral distribution of the core is presented separately in Figure 4, where the averaged spectral index is $\kappa_{\rm core} = 1.3 \pm 0.1$, which is roughly consistent with the linear fitting of core emission at different spws ($\kappa_{\rm core} = 1.4 \pm 0.1$, data points in Table 2).

Table 2 Gaussian Fitting of the Core Component at Each spw

spw (1)	Frequency (GHz) (2)	Majorax (arcsec) (3)	Minorax (arcsec) (4)	Pos Ang (°) (5)	Core flux (mJy) (6)
0	4.27	0.79	0.66	23	10.4 ± 0.13
1	4.40	0.76	0.62	39	9.4 ± 0.16
2	4.53	0.75	0.66	22	9.6 ± 0.13
3	4.65	0.74	0.61	38	9.4 ± 0.11
4	4.78	0.73	0.65	24	8.9 ± 0.13
5	4.91	0.77	0.65	30	8.7 ± 0.11
6	5.03	0.74	0.63	28	8.5 ± 0.11
7	5.17	0.69	0.55	15	8.4 ± 0.10
8	5.29	0.68	0.54	13	7.8 ± 0.10
9	5.42	0.68	0.53	17	7.6 ± 0.09
10	5.55	0.68	0.54	13	7.3 ± 0.08
11	5.68	0.71	0.61	8	7.1 ± 0.08
12	5.81	0.67	0.59	28	6.7 ± 0.08
13	5.93	0.73	0.68	35	6.4 ± 0.09

Column (1) represents the spw ID, Col. (2) displays the central frequency of each spw, Cols. (3) and (4) provide the major and minor axes of the Gaussian fitting respectively, Col. (5) lists the position angle and Col. (6) features the integrated core flux of the Gaussian component.

Her A has two bright radio lobes and a weak core. We present the relation between 178 MHz radio luminosity and [O III] luminosity for Her A and compare it with a sample of FR I and FR II radio galaxies in Figure 5, where the data on other FR I/II sources are selected from Fan & Wu (2019) and the data on Her A from Kellermann et al. (1969) and Buttiglione et al. (2009). It can be found that Her A deviates from other sources evidently in the $L_{\rm [O\ III]} - L_{\rm 178\ MHz}$ relation (open star in Fig. 5). Assuming the spectral index of $\kappa_{\rm core} = 1.3$ as derived from the core spectrum, we estimate the 178 MHz radio luminosity of the radio core, which is $L_{\rm core,178\,MHz} = 10^{32.6}\,{\rm erg\,Hz^{-1}\,s^{-1}}$. We find that radio emission of the core roughly follows the $L_{\rm [O\ III]} - L_{\rm 178\,MHz}$ relation as defined by other FR I/II sources (solid circle in Fig. 5). Assuming $L_{\rm bol} = 3500\,L_{\rm [O\ III]}$ (Heckman et al. 2004), we estimated the bolometric luminosity of Her A, $L_{\rm bol} = 10^{44.0}\,{\rm erg\,s^{-1}}$. The bolometric Eddington ratio is $L_{\rm bol}/L_{\rm Edd} = 10^{-3.6}$ ($L_{\rm Edd} = 1.3 \times 10^{38}\,M_{\rm BH}/M_{\odot}\,{\rm erg\,s^{-1}}$). Based on the total 151 MHz radio emission of the jet, we estimate the jet power of Her A using the $P_{\rm jet} - L_{\rm 151\,MHz}$ relation that is presented in Godfrey & Shabala (2013), where $P_{\rm jet,total} = 10^{46.1}\,{\rm erg\,s^{-1}}$ and Eddington-scaled jet power $P_{\rm jet,total}/L_{\rm Edd} = 10^{-1.5}$. Since the jet may have died in the core region, we also estimate the jet power based on radio core emission. We find $P_{\rm jet,core} = 10^{44.2}\,{\rm erg\,s^{-1}}$ and $P_{\rm jet,core}/L_{\rm Edd} = 10^{-3.4}$.

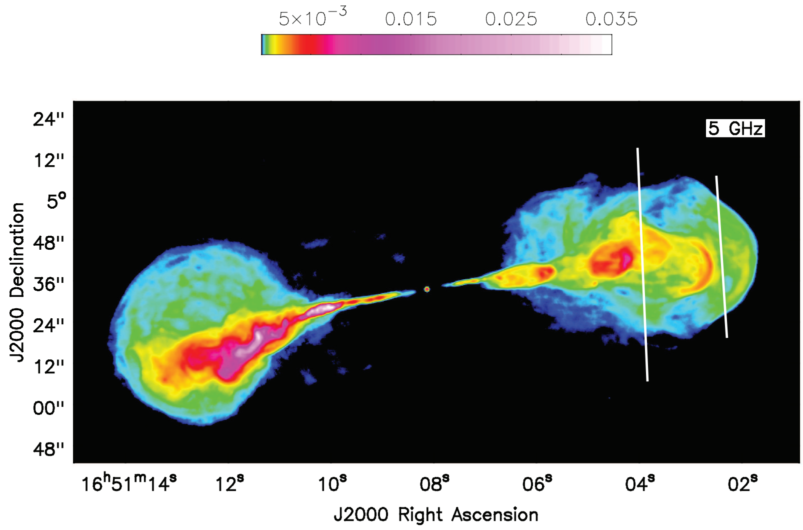

Fig. 1 The intensity distribution of Her A at 5 GHz, where the beam size is 0.73×0.70 arcsec and the color scale runs from 0.085 mJy beam^{-1} to 35.1 mJy beam^{-1}. The two *solid lines* represent the slices for analyzing the intensity distribution in one dimension.

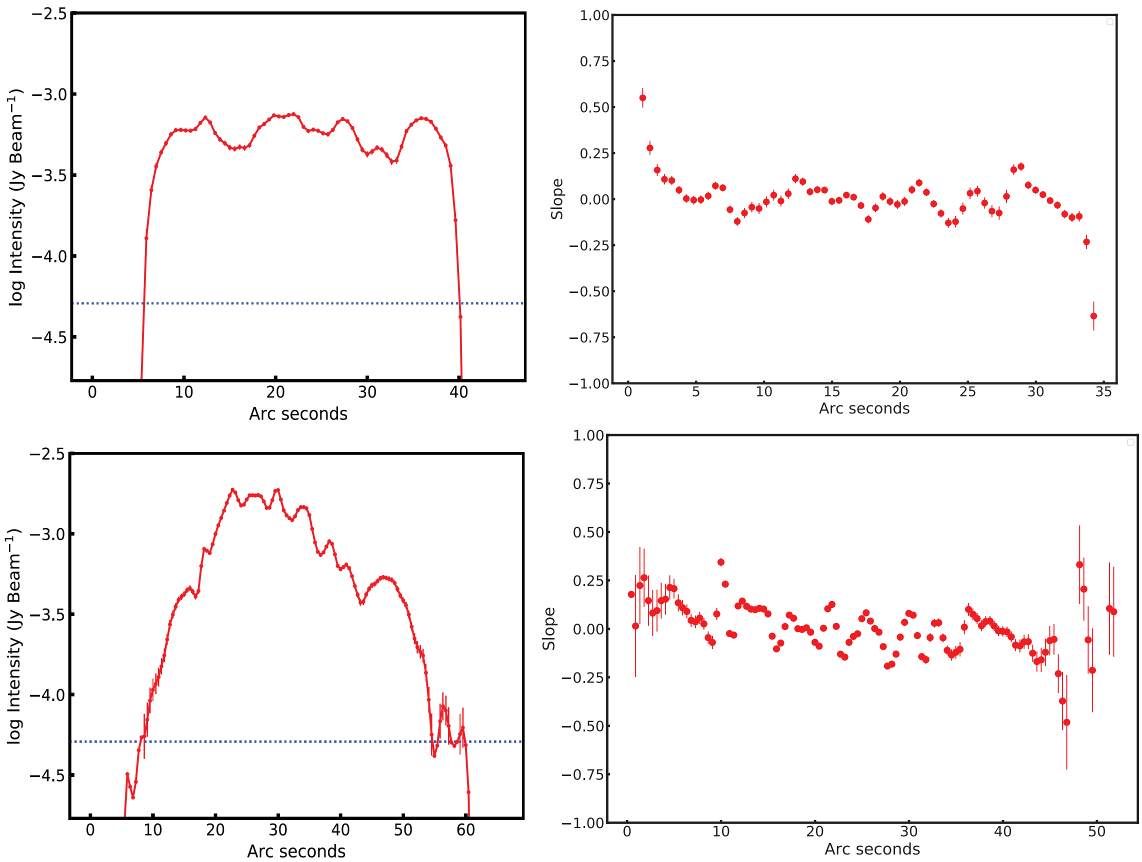

Fig. 2 The *upper* and *lower* panels represent the one dimensional intensity distribution for the two selected slices (*left*) and the corresponding slope of intensity variation against distance with the interval of 0.4 arcsec (*right*). The slope of intensity variation is calculated when the intensity is above the $3\,\sigma_{\rm I}$ levels (*dotted lines* in left panels).

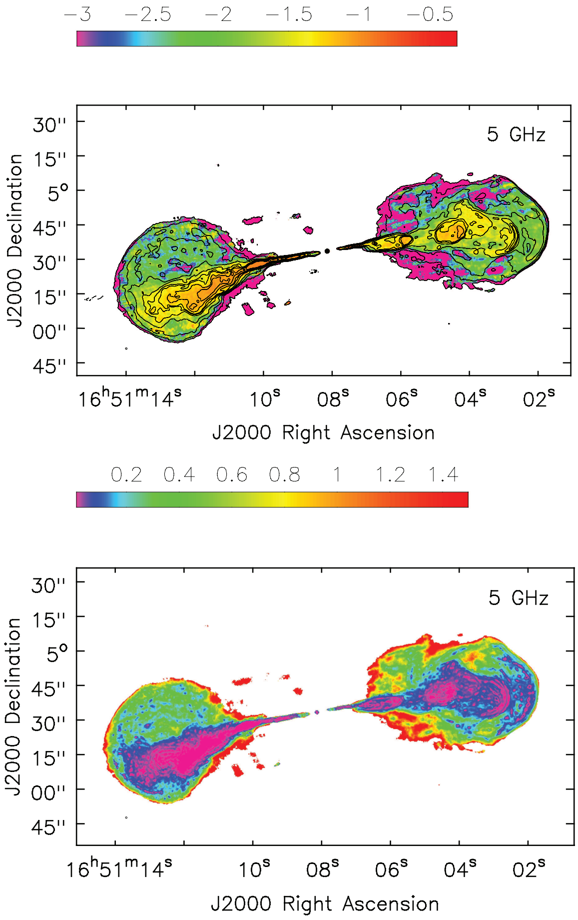

Fig. 3 The distributions of radio spectral index of Her A (*upper panel*) and its error (*lower panel*) which overlap with intensity contours map in the frequency range from 4.2–6.0 GHz. To decrease the error of the spectral index, the intensity above $5\sigma_I$ is considered. The beam size of both figures is 0.73×0.70 arcsec and the color scale runs from –3.0 to –0.3. Contours have the base level of $5\sigma_I$ and increase with a factor of 2.

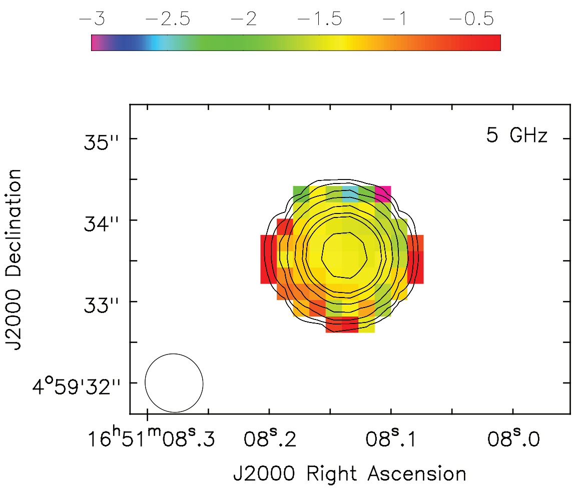

Fig. 4 Same as the *upper panel* of Fig. 3, but zoomed into the core region.

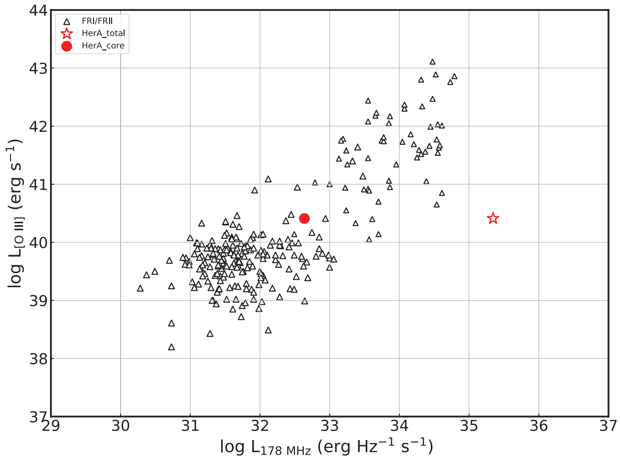

Fig. 5 The correlation between [O III] and 178 MHz radio luminosity for FR I and FR II sources, where the total and core radio luminosities of Her A are shown with *open star* and *solid circle* respectively. The other compared FR I/II sources are selected from Fan & Wu (2019) directly.

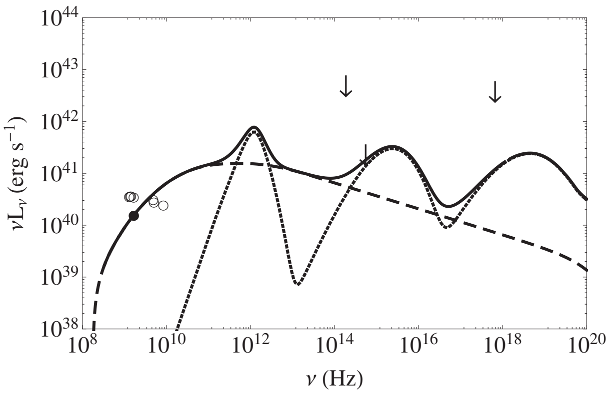

Fig. 6 The spectrum and model fitting with ADAF+jet model. The *dotted*, *dashed* and *solid lines* represent the ADAF, jet and total emission respectively. The *solid circle* and *open circles* represent the EVN and VLA data respectively. Radio core data are selected from Gizani & Garrett (2002), Gizani & Leahy (2003) and this work, near-infrared data are referenced from Madrid et al. (2006), and optical and X-ray core data are adopted from Balmaverde et al. (2006). Here we take the infrared to X-ray data as upper limits.

According to the Eddington-scaled bolometric luminosity and jet power of the core region, the central SMBH of Her A should stay in a low state, indicating that it accretes through an ADAF. Fujita et al. (2016) estimated the Bondi accretion rate for Her A, which is $0.089\, M_{\odot}\mathrm{yr}^{-1}$ or $\sim 1.6 \times 10^{-3} \dot{M}_{\rm Edd}$ ($\dot{M}_{\rm Edd} = 2.28\, M_{\rm BH}/M_8\, M_{\odot}\, \mathrm{yr}^{-1}$, $M_8 = 10^8\, \mathrm{M}_{\odot}$). We investigate the properties of the central engines of Her A based on the ADAF and jet model. We refer the reader to Feng et al. (2016) and Wu et al. (2013) for more details. The global structure and dynamics of the ADAF in the general relativistic frame surrounding a spinning SMBH are considered, where we adopt a fast rotating BH with a dimensionless spin of $a_* = 0.99$ in this work. The accretion rate is described by $\dot{M} = \dot{M}_{\rm out}(R/R_{\rm out})^{p_{\rm w}}$, where $\dot{M}_{\rm out}$ is the accretion rate at the outer boundary, $R_{\rm out}$, and $p_{\rm w}$ is the wind parameter. In this work, we simply set $\dot{M}_{\rm out} = \alpha\dot{M}_{\rm bondi}$, where α is the viscosity coefficient with a typical value of 0.3 (Narayan et al. 1997; Esin et al. 1997; Liu & Taam 2013). The typical magnetic parameter $\beta = 0.5$ and the fraction of the turbulent dissipation that directly heats the electrons $\delta = 0.1$ are also adopted in this work (e.g., Yuan & Narayan 2014; Wu & Cao 2008). In modeling the inner jet emission from the core, we adopt a phenomenological jet model, where a small fraction of the accreting material, $\dot{M}_{\rm jet}$, in the ADAF is transferred into the vertical direction to form a jet. We calculate the jet radiation in the internal shock scenario, where shocks accelerate a fraction of the electrons, $\xi_{\rm e}$, into a power-law energy distribution with an index of p, where typical values of $\xi_{\rm e} = 0.05$ and $p = 2.5$ are adopted. In the jet, we adopt the energy density of the accelerated electrons, $\epsilon_{\rm e} = 0.06$, and the energy density of the amplified magnetic field $\epsilon_{\rm B} = 0.02$. For Her A, we simply assume the jet velocity of $v_{\rm jet} = 0.8c$, the jet viewing angle of $\theta_{\rm view} = 50^\circ$ (Gizani & Leahy 2003) and a typical jet opening angle of $\theta_{\rm jet} = 5^\circ$. Due to the limited observational data, we just allow two free parameters in our model, which are the wind parameter, $p_{\rm w}$, and the outflow rate, $\dot{M}_{\rm jet}$. In the SED modeling, we use the high-resolution EVN data, which are slightly lower than those observed by EVLA. In Figure 6, we present our modeling results, where $\dot{M}_{\rm jet} = 10^{-5.2}\,\dot{M}_{\rm Edd}$. There is no strong evidence for the accretion component from the spectrum since the low-resolution infrared, optical and X-ray data should be considered as the upper limits, and we present the ADAF spectrum with a typical wind parameter of $p_{\rm w} = 0.1$, and ADAF contribution will be less if $p_{\rm w}$ is larger.

4 DISCUSSION AND CONCLUSIONS

We analyze the data from EVLA observation of Her A at C band during 2010–2011. The structures of total intensity at C band are quite similar to those observed in the 1980s (Gizani & Leahy 2003). The intensity of the lobe front is smooth, which suggests that the magnetic field still plays an important role there, since Kelvin-Helmholtz (KH) instability or/and Rayleigh-Taylor (RT) instability will lead to substructures in the jet edge (Chandrasekhar 1961). The smooth edge of the Her A lobe may support the magnetohydrodynamic (MHD) scenario. Nakamura et al. (2008) explored a numerical model of Her A based on MHD simulations, and suggested that the magnetically dominated model can roughly reproduce the main observational features of Her A (e.g., polarization, size of lobe, etc.). The motion of electrically-charged particles will be limited by the magnetic field in the lobe and the magnetic field also suppresses some instabilities (e.g., Li et al. 2006; Nakamura et al. 2006; Gan et al. 2017), which could lead to a sharp intensity profile at the lobe edge. Therefore, the sharp decrease in the intensity at the lobe front supports the MHD jet model, where the hydrodynamic jet is normally more diffuse. We will carefully compare the intensity distributions, smoothness and polarization with the MHD simulations in a future work.

Her A has a very weak radio core with flux density of $\sim 8.8\,\rm mJy$ at 4.8 GHz, which is about 10% lower than the value of $9.9\,\rm mJy$ at the same band as reported in Gizani & Leahy (2003). It should be noted that the core is quite stable at the timescale of several months, where its variability is less than 1% and 3% at 4.8 GHz and 8.4 GHz respectively (Gizani & Leahy 2003). We found that the calibration source 3C 286 varies less than 2% during this period, and the radio core of Her A becomes a little bit weaker compared to that observed more than twenty years ago. It should be noted that the radio core has a very steep spectrum ($\kappa_{\rm core} \sim 1.3$), which is much steeper than other radio cores in both FR Is and FR IIs (e.g., Fan et al. 2011; Pei et al. 2019). The unusually steep spectra of the radio core and large-scale lobe should be due to cessation of the injection of fresh particles, and the jet in the core region is also in the stage of dying.

The [O III] luminosity of Her A is also quite weak, which evidently deviates from the $L_{\rm OIII}$ and $L_{178\,\rm MHz}$ relation as defined by other FR I and FR II sources. This result suggests that the core may have become weak recently, while the jet that formed millions of years ago on a large scale is still active. It is interesting to note that the radio core emission roughly follows the $L_{\rm [O\ III]} - L_{178\,\rm MHz}$ relation as defined by other FR I/II sources, where both the size of radio core and the [O III] narrow-emission-line region extends to kpc scale. Therefore, both the narrow emission line and radio core suggest that the BH activity indeed becomes much weaker now, while both accretion and ejection in Her A should have been very powerful millions of years ago. In this work, the 178 MHz radio emission of the core is estimated from the 5 GHz radio emission based on the spectral index as derived from the 4–6 GHz data. The slight change in spectral index will not affect the above conclusion.

Both the radio core emission and the low-excitation [O III] lines suggest that the central engine of Her A may become weak compared with millions of years ago, but the weakness is not caused by obscuration of the torus. Macconi et al. (2020) also found that some LE FR IIs are intrinsically weak and are less luminous than other HE FR IIs by exploring their X-ray properties. We tentatively model the nuclear spectrum with an ADAF-jet model, which is widely adopted in modeling the spectrum of low-luminosity AGNs (e.g., Wu et al. 2007, 2013, 2018; Yuan 2007; Xie et al. 2016; Feng et al. 2016; Almeida et al. 2018). The radio emission measured by the high resolution of EVN and EVLA should come from non-thermal synchrotron emission of the jet, and the synchrotron emission of the thermal electrons in ADAF contributes little to the radio emission (otherwise the ADAF will produce too much X-ray emission). The EVLA cannot resolve the Her A radio core, and the high-resolution EVN data are adopted in our modeling. The high-resolution multi-wave band data are preferred to further test our model.

Because there is no strong nuclear X-ray emission, we cannot constrain the ADAF contribution in the total spectrum. Based on the Bondi accretion rate, our modeling results suggest that the wind parameter $p_{\rm w} \sim 0.1$ or a little bit larger, which is consistent with the modeling of other low-luminosity AGNs (Yuan et al. 2003; Wu et al. 2013; Feng et al. 2016). It should be noted that the parameters of our ADAF-jet model are not well constrained based on the limited observational data, where the typical values of many parameters are adopted from former works even though it will not affect our conclusion. Future high-sensitivity hard X-ray observations will help us to better understand the properties of the central engine in Her A.

Acknowledgements We appreciate our referee for many constructive comments and suggestions. Q. Wu and L.-H. Wu are supported by the National Natural Science Foundation of China (NSFC; Grant Nos. U1931203, 11622324, 11573009). R.-S. Lu is supported by the Key Program of NSFC (Grant No. 11933007) and Research Program of Fundamental and Frontier Sciences, Chinese Academy of Sciences (Grant No. ZDBS-LY-SLH011). X. Fan is supported by NSFC (Grant No. 11947099). J.-C. Feng is supported by the Science and Technology Foundation of Guizhou Province (QKHJC[2020]1Y018).

References

Almeida, I., Nemmen, R., Wong, K.-W., Wu, Q., & Irwin, J. A. 2018, MNRAS, 475, 5398
Balmaverde, B., Capetti, A., & Grandi, P. 2006, A&A, 451, 35
Best, P. N., & Heckman, T. M. 2012, MNRAS, 421, 1569
Buttiglione, S., Capetti, A., Celotti, A., et al. 2009, A&A, 495, 1033
Buttiglione, S., Capetti, A., Celotti, A., et al. 2010, A&A, 509, A6
Buttiglione, S., Capetti, A., Celotti, A., et al. 2011, A&A, 525, A28
Casadio, C., Marscher, A. P., Jorstad, S. G., et al. 2019, A&A, 622, A158
Chandrasekhar, S. 1961, Hydrodynamic and hydromagnetic stability (Oxford: Clarendon)
Chen, Y., Zhang, X., Zhang, H., et al. 2015, Ap&SS, 357, 100
Clausen-Brown, E., Lyutikov, M., & Kharb, P. 2011, MNRAS, 415, 2081
Diehl, S., Li, H., Fryer, C. L., & Rafferty, D. 2008, ApJ, 687, 173
Dreher, J. W., & Feigelson, E. D. 1984, Nature, 308, 43
Esin, A. A., McClintock, J. E., & Narayan, R. 1997, ApJ, 489, 865
Fan, J.-H., Yang, J.-H., Pan, J., & Hua, T.-X. 2011, RAA (Research in Astronomy and Astrophysics), 11, 1413
Fan, X.-L., & Wu, Q. 2019, ApJ, 879, 107
Fanaroff, B. L., & Riley, J. M. 1974, MNRAS, 167, 31P
Feng, J., Wu, Q., & Lu, R.-S. 2016, ApJ, 830, 6
Fujita, Y., Kawakatu, N., & Shlosman, I. 2016, PASJ, 68, 26
Gan, Z., Li, H., Li, S., & Yuan, F. 2017, ApJ, 839, 14
Ghisellini, G., & Celotti, A. 2001, A&A, 379, L1
Gizani, N. A. B., & Garrett, M. A. 2002, in Proceedings of the 6th EVN Symposium, 159
Gizani, N. A. B., & Leahy, J. P. 2003, MNRAS, 342, 399
Gizani, N. A. B., & Leahy, J. P. 2004, MNRAS, 350, 865
Godfrey, L. E. H., & Shabala, S. S. 2013, ApJ, 767, 12
Gopal-Krishna, & Wiita, P. J. 2000, A&A, 363, 507
Hardee, P. E., & Rosen, A. 2002, ApJ, 576, 204
Heckman, T. M., Kauffmann, G., Brinchmann, J., et al. 2004, ApJ, 613, 109
Kataoka, J., & Stawarz, Ł. 2005, ApJ, 622, 797
Kellermann, K. I., Pauliny-Toth, I. I. K., & Williams, P. J. S. 1969, ApJ, 157, 1
Kronberg, P. P., Lovelace, R. V. E., Lapenta, G., & Colgate, S. A. 2011, ApJL, 741, L15
Laing, R. A. 1981, ApJ, 248, 87
Laing, R. A., Jenkins, C. R., Wall, J. V., & Unger, S. W. 1994, Spectrophotometry of a Complete Sample of 3CR Radio Sources: Implications for Unified Models, in Astronomical Society of the Pacific Conference Series, 54, The Physics of Active Galaxies, eds. G. V. Bicknell, M. A. Dopita, & P. J. Quinn, 201
Laing, R. A., Canvin, J. R., Bridle, A. H., & Hardcastle, M. J. 2006, MNRAS, 372, 510
Li, H., Lapenta, G., Finn, J. M., Li, S., & Colgate, S. A. 2006, ApJ, 643, 92
Liu, B. F., & Taam, R. E. 2013, ApJS, 207, 17
Macconi, D., Torresi, E., Grandi, P., Boccardi, B., & Vignali, C. 2020, MNRAS, 493, 4355
Madrid, J. P., Chiaberge, M., Floyd, D., et al. 2006, ApJS, 164, 307

McKinney, J. C., & Narayan, R. 2007, MNRAS, 375, 513
McMullin, J. P., Waters, B., Schiebel, D., Young, W., & Golap, K. 2007, CASA Architecture and Applications, in Astronomical Society of the Pacific Conference Series, 376, Astronomical Data Analysis Software and Systems XVI, eds. R. A. Shaw, F. Hill, & D. J. Bell, 127
Nakamura, M., Li, H., & Li, S. 2006, ApJ, 652, 1059
Nakamura, M., Tregillis, I. L., Li, H., & Li, S. 2008, ApJ, 686, 843
Narayan, R., & Yi, I. 1994, ApJL, 428, L13
Narayan, R., & Yi, I. 1995, ApJ, 444, 231
Narayan, R., Kato, S., & Honma, F. 1997, ApJ, 476, 49
Pei, Z.-Y., Fan, J.-H., Bastieri, D., Sawangwit, U., & Yang, J.-H. 2019, RAA (Research in Astronomy and Astrophysics), 19, 070
Persic, M., & Rephaeli, Y. 2019, MNRAS, 490, 1489
Persic, M., & Rephaeli, Y. 2020, MNRAS, 491, 5740
Prior, C., & Gourgouliatos, K. N. 2019, A&A, 622, A122
Shakura, N. I., & Sunyaev, R. A. 1973, A&A, 500, 33
Stawarz, Ł., Siemiginowska, A., Ostrowski, M., & Sikora, M. 2005, ApJ, 626, 120
Tchekhovskoy, A., & Bromberg, O. 2016, MNRAS, 461, L46
Urry, C. M., & Padovani, P. 1995, PASP, 107, 803
Wang, J. M., Ho, L. C., & Staubert, R. 2003, A&A, 409, 887
Wu, Q., Yuan, F., & Cao, X. 2007, ApJ, 669, 96
Wu, Q., & Cao, X. 2008, ApJ, 687, 156
Wu, Q., Cao, X., Ho, L. C., & Wang, D.-X. 2013, ApJ, 770, 31
Wu, Q., Feng, J., & Fan, X. 2018, ApJ, 855, 46
Xie, F.-G., Zdziarski, A. A., Ma, R., & Yang, Q.-X. 2016, MNRAS, 463, 2287
Xu, Y.-D., Cao, X., & Wu, Q. 2009, ApJL, 694, L107
Yuan, F., Quataert, E., & Narayan, R. 2003, ApJ, 598, 301
Yuan, F. 2007, Advection-dominated Accretion: From Sgr A* to Other Low-luminosity AGNs, in Astronomical Society of the Pacific Conference Series, 373, The Central Engine of Active Galactic Nuclei, eds. L. C. Ho, & J. W. Wang, 95
Yuan, F., & Narayan, R. 2014, ARA&A, 52, 529
Yuan, F., Gan, Z., Narayan, R., et al. 2015, ApJ, 804, 101
Zhang, H., Chen, X., Böttcher, M., Guo, F., & Li, H. 2015, ApJ, 804, 58